Generation of Coherent Broadband Photon Pulses with a Cascaded Longitudinal Space-Charge Amplifier

A. Marinelli, E. Hemsing, M. Dunning, D. Xiang, S. Weathersby, F. O'Shea, I. Gadjev, C. Hast, and J. B. Rosenzweig

Phys. Rev. Lett. **110**, 264802 — Published 27 June 2013

DOI: 10.1103/PhysRevLett.110.264802

Generation of Coherent Broadband Photon Pulses with a Cascaded Longitudinal Space-Charge Amplifier

A. Marinelli,[1] E. Hemsing,[2] M. Dunning,[2] D. Xiang,[2] S. Weathersby,[2]
F. O'Shea,[1] I. Gadjev,[1] C. Hast,[2] and J. B. Rosenzweig[1]

[1]*Department of Physics and Astronomy, University of California Los Angeles, Los Angeles, CA 90095, USA*
[2]*SLAC National Accelerator Laboratory, Menlo Park, California 94025, USA*

The longitudinal space-charge amplifier has been recently proposed as an alternative to the free electron laser instability for the generation of intense broad-band radiation pulses (*Phys. Rev. ST Accel. Beams 13, 110701 (2010)*). In this Letter we report on the experimental demonstration of a cascaded longitudinal space-charge amplifier at optical wavelengths. Although seeded by electron beam shot-noise, the strong compression of the electron beam along the three amplification stages leads to emission of coherent undulator radiation pulse exhibiting a single spectral spike and a single transverse mode. The on-axis gain is estimated to exceed four orders of magnitude with respect to spontaneous emission.

The successful lasing of the LCLS [1] and SACLA [2] free-electron lasers (FELs) has established the high-gain FEL as the brightest source of monochromatic, hard x-rays, allowing the exploration of nature with unprecedented temporal and spatial resolution [3, 4]. While the narrow bandwidth of FELs is a desirable feature in applications such as imaging and spectroscopy, it ultimately limits the ability of the FEL to generate few-cycle pulses for ultra-fast experiments. As an alternative, the longitudinal space-charge amplifier (LSCA) has recently been proposed as a powerful broad-band coherent radiation source [5]. In a LSCA, a relativistic electron beam (e-beam) becomes modulated in density (i.e, microbunched) by the interaction with its own collective space-charge forces, combined with longitudinal dispersion in transport. This microbunching instability process was first identified as a detrimental effect in the context of FEL injectors [6–12]. However, as pointed out in [5], it can be optimized and cascaded through several amplification stages to yield strong microbunching for the emission of intense broad-band coherent light. Due to its unique spectral properties, the LSCA is a natural candidate for the generation of intense attosecond radiation pulses [13]. Furthermore, the LSCA presents several advantages in terms of compactness and robustness to non-ideal beam conditions.

In this Letter, we report on the experimental demonstration of the LCSA as a new type of broadband, fully coherent radiation source at the Next Linear Collider Test Accelerator (NLCTA) of the SLAC National Accelerator Laboratory. Our experimental setup is shown in Figure 1, and exploits the existing three-chicane echo-enabled, harmonic generation seeding beamline [14, 15] as a cascaded three-stage LSCA seeded by shot-noise. Through the proper tuning of the bunch compression, we demonstrate the generation of an intense, single mode pulse with an intensity gain of four orders of magnitude over the spontaneous emission level.

The physical mechanism of the space-charge instability can be modeled as a two-step process. An e-beam with an initial density perturbation at the longitudinal spatial frequency k travels through a transport channel (drift) of length L_d. During transport, the modulated longitudinal space-charge fields induce a corresponding energy modulation in the e-beam. Afterwards, the electrons travel through a longitudinally dispersive transport element (e.g, a magnetic bending chicane) which transforms the energy modulation back into a density modulation, but with an amplitude larger than the initial value. This process can start from shot-noise or from a coherent microbunching induced by interaction with an external laser, and can be repeated in several amplification stages to enhance the density modulation amplitude.

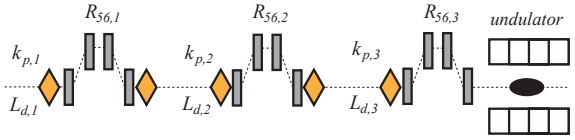

FIG. 1: Overview of the beam-line for the NLCTA experiment. Three chicanes separate three drift sections within a FODO lattice defined by quads (diamonds).

The microbunching instability has been investigated in detail elsewhere [9–12, 16]. To provide a dynamical description of the cascaded LSCA setup explored experimentally here, it is useful to follow the matrix formalism of Gover et al. [17] for a simple one-dimensional (1D), cold beam model. The beam density modulation can be quantified by the beam bunching factor, given by $b = \sum_n \exp(-ikz_n)/N$, where z_n is the longitudinal position of the n_{th} particle and N is the number of particles. The energy modulation is defined similarly as $\mu = \sum_n \eta_n \exp(-ikz_n)/N$, where $\eta_n = \delta\gamma_n/\gamma$ is the relative energy deviation and γ the beam's Lorentz factor. In the linear approximation (i.e. when $b \ll 1$) for a single-stage LSCA, the evolution of the two collective variables (b, μ) under the influence of space-charge forces and dis-

persion is described by the transport matrix:

$$\begin{pmatrix} b_1 \\ \mu_1 \end{pmatrix} = \mathbf{RM} \begin{pmatrix} b_0 \\ \mu_0 \end{pmatrix}. \quad (1)$$

where $\mathbf{M} = \begin{pmatrix} \cos(k_p L_d) & -\frac{ik}{\gamma^2 k_p}\sin(k_p L_d) \\ \frac{k_p \gamma^2}{ik}\sin(k_p L_d) & \cos(k_p L_d) \end{pmatrix}$ is the space-charge evolution matrix, $k_p = \sqrt{\frac{e^2 n_0}{\epsilon_0 m c^2 \gamma^3}}$ is the relativistic spatial plasma frequency, n_0 is the beam density, e the electron charge, ϵ_0 is the vacuum permittivity, m the electron mass, and c the speed of light. The linear transport through the chicane is described by the transport matrix $\mathbf{R} = \begin{pmatrix} 1 & -ikR_{56} \\ 0 & 1 \end{pmatrix}$, where R_{56} is the longitudinal dispersion in the chicane. In general, if N_s amplification stages are used in series, the final variables can be computed by simple chain multiplication of the evolution matrices in each stage:

$$\begin{pmatrix} b_{N_s} \\ \mu_{N_s} \end{pmatrix} = \mathbf{R_{N_s} M_{N_s}} \ldots \mathbf{R_2 M_2 R_1 M_1} \begin{pmatrix} b_0 \\ \mu_0 \end{pmatrix}. \quad (2)$$

The gain in the l^{th} section is then defined as $g_l = b_l / b_{l-1}$. Assuming that the amplification process starts from a beam with negligible initial energy modulation ($\mu_0 = 0$), use of the single stage evolution matrix yields the microbunching gain,

$$g_1 = b_1/b_0 = \cos(k_p L_d) - \gamma^2 R_{56} k_p \sin(k_p L_d). \quad (3)$$

Under conditions of high gain ($|g_1| \gg 1$), the $\cos(k_p L_d)$ term can be neglected and the gain is proportional to the longitudinal dispersion in the chicane, $g_1 \simeq -\gamma^2 R_{56} k_p \sin(k_p L_d)$. The overall gain in a cascaded system is given by the product of the microbunching gain in each stage,

$$g = g_1 g_2 \ldots g_{N_s} = b_{N_s}/b_0. \quad (4)$$

Note that this formula is only valid if a significant amount of energy modulation is developed in each stage. Consider the simplified case of a two-stage LSCA ($N_s = 2$). In the high-gain approximation, the gain at the exit of the second stage is $g_2 \simeq \gamma^4 R_{56,1} k_{p,1} \sin(k_{p,1} L_{d,1}) R_{56,2} k_{p,2} \sin(k_{p,2} L_{d,2})$. On the other hand, if no energy modulation is developed in the second drift (namely if $k_{p,2} L_{d,2} \to 0$), then the two-stage gain formula from Eq (2) reduces to $g_2 \simeq \cos(k_{p,1} L_{d,1}) - \gamma^2 (R_{56,1} + R_{56,2}) k_{p,1} \sin(k_{p,1} L_{d,1})$. The latter is essentially the single stage formula in Eq. (3), where the energy modulation from the first stage is converted into a density modulation by the sum total dispersion from each stage. Note that the microbunching still grows from one stage to the next, but the gain is additive rather than multiplicative. We will therefore refer to the first case as *cascaded* microbunching gain, and to the second case as *additive* microbunching gain. The distinct advantage of the cascaded arrangement is the potential for much larger gain for the same total dispersion. This concept can be generalized to multiple stages, and the signature of cascading is that the gain is dependent on the way the total R_{56} is partitioned.

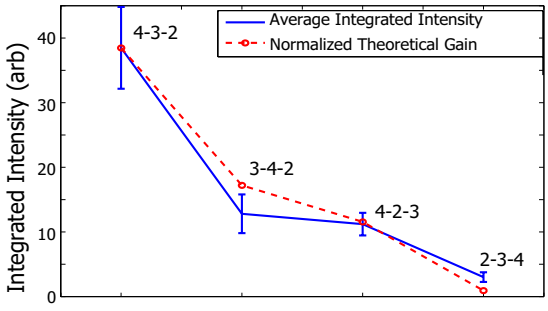

FIG. 2: Integrated camera intensity for three different R_{56} (marked in mm for C1-C2-C3, respectively) configurations, total $R_{56} = 9$ mm. For comparison the theoretical microbunching power gain is shown, normalized to the first experimental point. The error bars represent the uncertainty on the mean intensity ($\pm 3\sigma$) averaged over 250 shots.

The 1D theory can be easily modified to include 3D effects, energy spread and beam compression. Following the approach of [18], it can be shown that the plasma frequency for a cold beam is given by replacing $k_p \to k_p^{(3D)} = k_p \Omega$, where $\Omega < 1$ is the normalized plasma frequency, which accounts for the finite size of the e-beam and transverse betatron motion. The explicit dependence of Ω depends on the transverse beam distribution that one considers (see e.g. [9, 19]). In general, Ω is a decreasing function of the 3D parameter $D = k\sigma_x/\gamma$, where σ_x is the beam rms transverse size. For a transversely laminar e-beam we have that $\Omega \to 1$ for $D \gg 1$ while $\Omega \to 0$ for $D \ll 1$, and thus microbunching gain is suppressed by 3D effects for long wavelengths. At short wavelengths, on the other hand, the gain process is dominated by energy-spread effects, according to an exponential suppression factor $\exp(-(k\sigma_\eta R_{56})^2/2)$ for a beam with a gaussian relative energy spread σ_η. Finally, in the presence of a linear energy chirp, the effect of wavelength compression during dispersion has to be taken into account. For a given linear energy chirp $h = \frac{d\gamma}{\gamma dz}$, the wavelength changes as $\lambda \to \lambda/C$, where $C = 1/(1 + hR_{56})$. The gain formula then has to be modified as:

$$g_1 = \left(\cos(k_p^{(3D)} L_d) - C\gamma^2 R_{56} k_p^{(3D)} \sin(k_p^{(3D)} L_d)\right) \times \exp\left(-\frac{(Ck\sigma_\eta R_{56})^2}{2}\right) \quad (5)$$

where k is the microbunching frequency before the chi-

cane and Ck is the frequency after the chicane. With this expression, the total gain in a cascaded LSCA can be computed from the product in Eq. (4), taking into account the wavelength shift due to compression, as well as the corresponding R_{56}, $k_p^{(3D)}$ and L_d in each stage.

The cascaded LSCA experimental setup shown in Fig. 1 is composed of three-magnetic chicanes each separated by drifts, with an undulator used as a radiator after the final chicane. The e-beam is generated by an S-band photoinjector and accelerated as high as 120 MeV by two X-band accelerating structures (named linac 0 and linac 1). The three-magnetic chicanes (C1, C2 and C3) have tunable longitudinal dispersion in the range 0.8 mm $< R_{56} <$ 10 mm. The radiator employed is a helical undulator with N_w=11 periods of length $\lambda_w = 1.9$ cm and an undulator parameter $K = 0.58$. The operating beam energy in this experiment was 72 MeV (γ=141), corresponding to a resonant emission wavelength of $\lambda_r =$ 640 nm. Beam compression was achieved by operating linac 0 on crest at an energy of 35 MeV and varying the phase of linac 1 forward of crest. The space-charge interaction evolves as follows. Before C1, most of the interaction happens in a drift of length $L_{d,1} = 10$ m where the beam has an average beam size of $\sigma_{x,1} = 220$ μm, while the drifts between C1 and C2, and C2 and C3 have lengths of $L_{d,2} = L_{d,3} = 2$ m with a beam size of $\sigma_{x,2}$ = 160 μm and $\sigma_{x,3} = 150$ μm, respectively. The initial beam current is $\simeq 10 Amps$, with an uncorrelated energy-spread of $\sigma_E \simeq 1.5 keV$. The space-charge instability is seeded by shot-noise, which gives a broadband initial microbunching power of $< |b_0|^2 >= 1/N$.

To explore cascaded amplification, the coherent undulator radiation intensity was measured for different R_{56} configurations, each yielding the same total dispersion of 9 mm. Figure 2 shows the integrated undulator radiation signal measured with a near-field camera, as well as a comparison with the theoretical prediction for the 3D microbunching gain, calculated under the assumptions of three-stage cascaded gain, a gaussian transverse distribution and linear compression, using the measured beam parameters. For ease of comparison, the radiation intensity for the theoretical curve is normalized to the first experimental point. The plot shows good agreement between the measured and predicted intensity variation with different chicane dispersions.

Due to the x-band accelerating field curvature, the global chicane compression results in a high-current leading spike. Figure 3 shows the result of a one-dimensional particle transport simulation performed with the "LOSCA" approach described in Ref. [13]. For a strongly compressed bunch, the microbunching gain is confined to the leading current peak, resulting in the emission of a pulse notably shorter than the total bunch length; conversely, for moderate compression the length of the microbunched fraction of the bunch is comparable to the entire bunch length. Figure 4 shows typical single-shot coherent undulator radiation spectrometer images from the LSCA with $R_{56,1} = 4$ mm, $R_{56,2} = 2.5$ mm, $R_{56,3} = 1.5$ mm for two scenarios: moderate gain (phase of linac 1 $\phi_1 \simeq 35°$), and maximum gain ($\phi_1 \simeq 39°$). The observed angular and spectral structure of the coherent radiation can be understood by examination of the far-field differential spectrum of the helical undulator,

$$\frac{dU}{dkd\Omega_s} = \frac{dU}{dkd\Omega_s}\Big|_{sp} N^2 |B(\vec{k})|^2, \qquad (6)$$

where Ω_s is the solid angle and $\frac{dU}{dkd\Omega_s}\big|_{sp}$ is the single-particle differential spectrum [20]. The form factor $B(\vec{k}) = \frac{1}{N}\sum_j exp(-i\vec{k}\cdot\vec{x}_j)$ is the 3D Fourier transform of the charge distribution, where the forward angle is $\theta = \cos^{-1}\frac{k_x^2+k_y^2}{k_x^2+k_y^2+k_z^2}$. At a given angle θ, electrons traversing the undulator emit near the wavelength $\lambda_r = \lambda_w\left(1+K^2+\gamma^2\theta^2\right)/2\gamma^2$ with a FWHM spectral bandwidth of $\delta\lambda/\lambda \simeq 1/N_w$. If the instability is seeded by shot-noise, the microbunching spectrum is composed of several uncorrelated spikes with relative width given roughly by $\delta\lambda_{spike}/\lambda \simeq \lambda/L_b$, where L_b corresponds to the length of the microbunched distribution. Note that L_b can be shorter than the actual length of the e-beam if a leading current peak dominates the microbunching process (see Fig. 3, red curve). If the bandwidth of the undulator is larger than the bandwidth of a single spectral spike, the coherent radiation spectrum from the LSCA shows several uncorrelated spikes. This corresponds to the slippage length in the undulator $L_s = N_w\lambda_r$ being shorter than the length L_b of the density modulated fraction of the bunch (see Fig. 3, red curve). In the opposite case, if the slippage length is longer than the microbunching structure ($L_s > L_b$), the radiation spectrum is characterized by a single coherent spike composed of $\sim N_w$ optical cycles. These cases are borne out from the measurements in Fig. 4. The intermediate gain configuration (left) corresponds to a weaker current compression than the peak gain. For this value of compression, the spectrum exhibits a spiky structure, as the slippage length in the undulator is shorter than the fraction of the e-beam contributing to coherent emission. In the optimal compression case (right), the microbunched fraction of the e-beam becomes shorter than the slippage length, and the emission is characterized by a single spectral spike. The measured on-axis FWHM bandwidth of the coherent emission distribution is $\Delta\lambda_r/\lambda_r \simeq 9\%$, in agreement with the on-axis emission bandwidth of the undulator. The measured angular integrated spectrum has a wider bandwidth $\Delta\lambda_r/\lambda_r \simeq 14\%$ since longer wavelengths are emitted off-axis.

For moderate compression the radiation intensity distribution also exhibits speckles in the transverse dimension, while for stronger compression, a single, coherent transverse mode is observed (see the intensity depen-

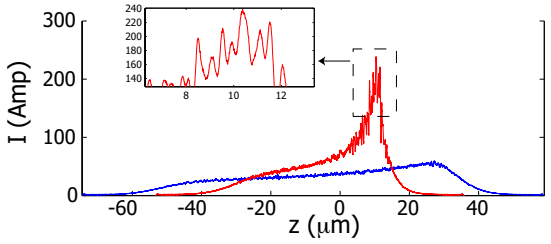

FIG. 3: Simulated beam current profile for a moderately compressed beam (blue line, $\phi_1 \simeq 35^\circ$) and for a strongly compressed beam (red line, $\phi_1 \simeq 39^\circ$).

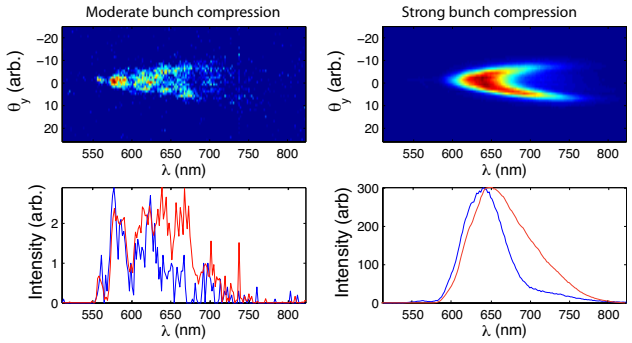

FIG. 4: Single-shot spectrometer image (upper images), on-axis spectrum (lower images, blue line) and integrated spectrum (lower images, red lines) from a strongly compressed beam (right images) and for moderate compression (left images).

dence on θ_y in the upper images in Fig. 4). This behavior is anticipated from theoretical predictions [19]. The transverse space-charge eigenmodes of a laminar beam are fully degenerate for large values of the 3D parameter $D = k\sigma_x/\gamma$, i.e. for short wavelengths. As a consequence of the full degeneracy, the transverse distribution of microbunching in this limit is composed of several uncorrelated speckles [12, 16], resulting in the emission of a transversely incoherent mode in the radiator. This effect limits the operation of an un-chirped LSCA to wavelengths $\lambda > 2\pi\sigma_x/\gamma$ for transverse coherence. For the typical operating condition of the NLCTA, this is in the mid-infrared. The observed transition to transverse coherence was therefore obtained as a consequence of bunch compression. For the case of strong compression, the optical microbunching generated at the last stage of the LSCA is the result of long-wavelength microbunching amplified in the first stage and frequency up-shifted to optical wavelengths by compression in the second and third chicanes. As a result the beam radiates a single coherent transverse mode in the undulator, as shown in Figure 5.

Finally, to accurately measure the integrated intensity gain, we used a high dynamic range photodiode detector. With $12pC$ of total beam charge, the average gain in the

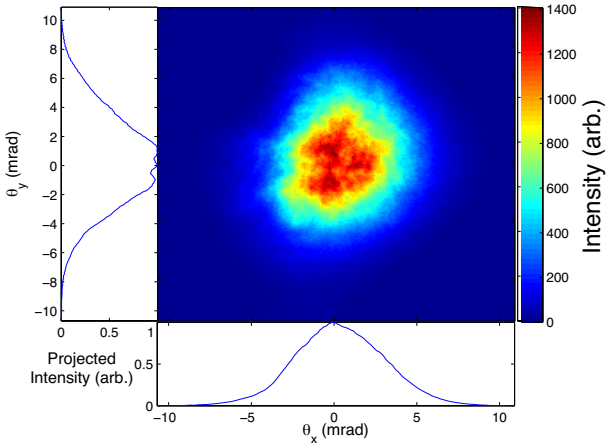

FIG. 5: Far-field undulator radiation image and projected intensity in θ_x and θ_y at maximum compression.

integrated intensity over the spontaneous emission background was measured to be $U_{max}/U_{inc} \simeq 600 \pm 30$, with a shot-to-shot intensity fluctuation of $\sigma_U/U_{inc} = 480$. The e-beam form factor $B(\vec{k})$ decays rapidly for angles larger than the coherent angle $\theta_c > \lambda_r/2\pi\sigma_x$, while the width of the spontaneous undulator radiation is $\theta_{sp} \simeq (1 + K^2)^{1/2}/\gamma$. For the typical operating conditions in our experiments $\theta_{sp} > \theta_c$, which means that the angular width of the coherent radiation is dominated by the geometry of the e-beam. Since the angular width of the incoherent far-field distribution is measured to be 2.2 times larger than that of the coherent distribution, the on-axis intensity gain is significantly higher, approximately 3000. Furthermore, only a fraction of the e-beam contributes to the coherent emission, while the entire e-beam contributes to incoherent emission. From the numerical simulations we estimate that the current peak that drives the microbunching process contains roughly 20% of the bunch charge. It follows that the peak power emitted on-axis can be estimated to be four orders of magnitude above the shot-noise level [21].

In conclusion, in this Letter we have discussed the first experimental demonstration of a cascaded LSCA. In our experiment, the space-charge microbunching instability was controlled and optimized to generate intense broadband coherent undulator radiation pulses. Strong bunch compression due to a chirped beam results in coherent radiation pulses with a single transverse mode, consistent with our theoretical understanding of the amplification and compression processes. Due to the short duration of the current peak, a single spectral mode has been observed under conditions of strong compression. Finally, the cascading process enabled by use of three chicanes has been investigated by scanning the relative values of the three R_{56}s while keeping the total compression constant. This experiment provides a proof-of-principle demonstra-

tion for the generation of broad-band coherent radiation at fourth generation light sources, and potentially extends the operation of FEL user facilities into new and unexplored regimes.

The authors would like to acknowledge G. Morales, Z. Huang and P. Musumeci for useful discussions and suggestions. This research is supported by grants from US DOE Contract Nos. DE-FG02-07ER46272 and DE-FG03-92ER40693, Office of Naval Research Contract No. N00014-06-1-0925, DARPA Contract No. N66001-11-4197 and DOE Contract No. DE-AC02-76SF00515.

[1] P. Emma et al., Nat Photon **4**, 641 (2010).
[2] T. Ishikawa, H. Aoyagi, T. Asaka, and al., Nat Photon **6**, 540 (2012).
[3] H. N. Chapman, P. Fromme, A. Barty, T. A. White, R. A. Kirian, and al., Nature **470**, 73 (2011).
[4] M. M. Seibert, E. T., F. Maia, M. Svenda, and al., Nature **470**, 78 (2011).
[5] E. A. Schneidmiller and M. V. Yurkov, Phys. Rev. ST Accel. Beams **13**, 110701 (2010).
[6] H. Loos and et al, Proceedings of the 2008 Free-Electron Laser Conference (Gyeongju, Korea) p. p. 619 (2008).
[7] S. Wesch and et al, Proceedings of the 2009 Free-Electron Laser Conference (Liverpool, UK) p. 485 (2009).
[8] A. H. Lumpkin, Y. C. Chae, J. W. Lewellen, W. J. Berg, M. Borland, S. G. Biedron, R. J. Dejus, M. Erdmann, Z. Huang, K. J. Kim, et al., Nucl. Instrum. Meth. A **507**, 200 (2003).
[9] Z. Huang, M. Borland, P. Emma, J. Wu, C. Limborg, G. Stupakov, and J. Welch, Phys. Rev. ST Accel. Beams **7**, 074401 (2004).
[10] M. Borland, Y. Chae, P. Emma, J. Lewellen, V. Bharadwaj, and al., Nucl. Instrum. Meth. **483**, 268 (2002), ISSN 0168-9002.
[11] M. Venturini, Phys. Rev. ST Accel. Beams **11**, 034401 (2008).
[12] D. Ratner, A. Chao, and Z. Huang, Proceedings of the 2008 Free-Electron Laser Conference p. 338 (2008).
[13] M. Dohlus, E. A. Schneidmiller, and M. V. Yurkov, Phys. Rev. ST Accel. Beams **14**, 090702 (2011).
[14] D. Xiang, E. Colby, M. Dunning, S. Gilevich, C. Hast, K. Jobe, D. McCormick, J. Nelson, T. O. Raubenheimer, K. Soong, et al., Phys. Rev. Lett. **105**, 114801 (2010).
[15] D. Xiang, E. Colby, M. Dunning, S. Gilevich, C. Hast, K. Jobe, D. McCormick, J. Nelson, T. O. Raubenheimer, K. Soong, et al., Phys. Rev. Lett. **108**, 024802 (2012).
[16] A. Marinelli and J. B. Rosenzweig, Phys. Rev. ST Accel. Beams **13**, 110703 (2010).
[17] A. Gover and E. Dyunin, Phys. Rev. Lett. **102**, 154801 (2009).
[18] A. Marinelli, E. Hemsing, and J. B. Rosenzweig, Physics of Plasmas **19**, 063108 (pages 9) (2012).
[19] A. Marinelli, E. Hemsing, and J. Rosenzweig, Phys. Plasmas 18, 103105 (2011).
[20] B. M. Kincaid, Journal of Applied Physics **48**, 2684 (1977).
[21] We note that the local power gain estimated from the measurements (1.5×10^4) is in good agreement with the estimated microbunching power gain from the linear theory, which is $\simeq 2.5 \times 10^4$. However the results from the theory should be interpreted with care, since the total gain is strongly dependent on the local energy-chirp, which is influenced by effects such as wake-fields and zeroth order space-charge forces, that are not included in the model.